Earth Syst. Sci. Data, 14, 5617–5635, 2022
https://doi.org/10.5194/essd-14-5617-2022

Open Access Earth System Science Data

Deep-water hydrodynamic observations of two moorings sites on the continental slope of the southern Adriatic Sea (Mediterranean Sea)

Francesco Paladini de Mendoza[1], Katrin Schroeder[1], Leonardo Langone[2], Jacopo Chiggiato[1], Mireno Borghini[3], Patrizia Giordano[2], Giulio Verazzo[2], and Stefano Miserocchi[2]

[1]CNR-ISMAR, Arsenale Castello, 2737/F, 30122 Venice (VE), Italy
[2]CNR-ISP, Via P. Gobetti, 101, 40129 Bologna (BO), Italy
[3]CNR-ISMAR, Pozzuolo di Lerici, 19032 La Spezia, (SP), Italy

Correspondence: Francesco Paladini de Mendoza (francesco.mendoza@ve.ismar.cnr.it)

Received: 15 June 2022 – Discussion started: 7 July 2022
Revised: 12 November 2022 – Accepted: 15 November 2022 – Published: 20 December 2022

Abstract. This work presents an 8-years-long dataset of monitoring activities conducted on the western margin of the southern Adriatic Sea where two moorings have been placed since 2012 in sites that are representative of different morpho-dynamic conditions of the continental slope (open slope vs. submarine canyon). The dataset includes measurements conducted with both current meters and conductivity, temperature and depth (CTD) probes, and it provides information about the hydrodynamics and thermohaline properties of the last 100 m of the water column. The hydrodynamics in both sites are dominated by weak currents ($< 0.1\,m\,s^{-1}$) which undergo yearly to episodic pulsation able to exceed intensity greater than $0.5\,m\,s^{-1}$, which are linked to the passage of dense waters. The 8-years records presented here represent a starting point for the continuous observation activity set up on occasion of the "Operation Dense Water" in 2012 focussed on the southern Adriatic deep-water dynamics. Since then, the observatory has been ongoing since 2012 and the database is regularly updated. All the data described here are made publicly available from https://doi.org/10.5281/zenodo.6770201 (Paladini de Mendoza et al., 2022) and are compliant with the FAIR principles (findable, accessible, interoperable and reusable).

1 Introduction

The Adriatic Sea is a sub-basin of the eastern Mediterranean Sea, with unique characteristics from the geological and oceanographic points of view. The basin is enclosed between two mountain chains (the Apennines and Dinaric alps) to the west and to the east, and with an elongated shape (the axis is oriented from SE to NW), a length of 800 km and an average width of 180 km. In the south, the Adriatic Sea is connected with the Ionian Sea through the Strait of Otranto.

The southern Adriatic Margin was built during the last half million years and its structure is a result of eustatic depositional cycles and complex quaternary uplift and deformation patterns (Bertotti et al., 1999; Ridente and Trincardi, 2002), well summarised by Bonaldo et al. (2016). The north-western sector of the slope is constituted by the south Gargano system which is the main deformation zone that extends offshore with the Gondola Deformation Belt (GDB, see Fig. 1). In this sector, there is a complex bedforms system where large sediment drift and furrow field give evidence of a strong bottom currents activity (Minisini et al., 2006; Martorelli et al., 2010), and asymmetric upstream migrating mud-waves indicate a depositional environment (Verdicchio and Trincardi, 2006; Trincardi et al., 2007a, b; Verdicchio et al., 2007). To the south, the major conduit influencing off-shelf fluxes and deep circulation is provided by the Bari Canyon System engraved in the continental margin with two main branches with a total length of about 30 km along the W–E direction (Turchetto et al., 2007; Rubino et al., 2012). During the sea-level low stand of the last glacial maximum, sediments were

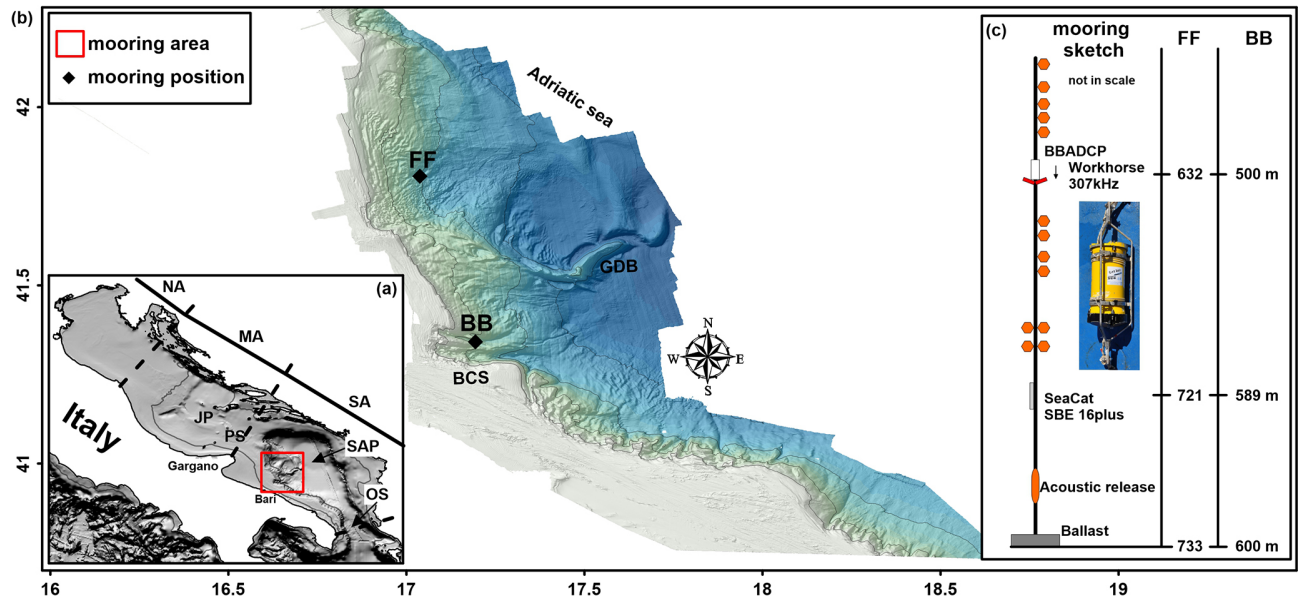

Figure 1. Study area. Panel **(a)** represents the Adriatic Sea divided by dotted lines in the three sub-sectors: north Adriatic (NA), middle Adriatic (MA) and south Adriatic. JP indicates Jabuka Pit, PS the Pelagosa Sill, SAP is south Adriatic Pit and OS is the Otranto Strait. The red box encloses the western margin where moorings are deployed, detailed in the panel; bathymetry is provided by EMODNET portal (https://portal.emodnet-bathymetry.eu/, last access: 7 December 2022) **(b)** where BB and FF are respectively the mooring site in the Bari Canyon System (BCS) and in the open slope. The GDB is the Gondola Deformation Belt. The panel **(c)** represents the sketch not in scale of mooring arrays.

supplied into the canyon directly from river deltas or longshore drift, but at present the canyon head is far from the coastal sediments and can be fed only by shelf currents or episodic density currents.

The Adriatic Sea is one of the three Mediterranean sites where density currents can be originated and are essentially of two types: the North Adriatic Dense Water (NAdDW), a cold and dense shelf water that forms in the northern sector during intense and cold outbreaks in winter (Hendershott and Malanotte-Rizzoli, 1976; Franco et al., 1982), and the Adriatic Deep Water (ADW) which forms by open ocean convection between late winter and early spring in the centre of the permanent cyclonic gyre of the southern Adriatic and vertically mixes the water column up to a variable depth (Vilibić and Orlić, 2002; Gačić et al., 2002; Manca et al., 2002; Civitarese et al., 2005).

In February 2012, the European region experienced a 2-week severe cold period that heavily impacted the northern Adriatic Sea. Immediately, a rapid response experiment called Operation Dense Water was conducted in the southern Adriatic to observe the dense water masses dynamics (Chiggiato et al., 2016b). These activities funded by the Italian research programme RITMARE (https://maritime-spatial-planning.ec.europa.eu/projects/la-ricerca-italiana-il-mare, last access: 7 December 2022) spanned from oceanographic modelling and physical and biogeochemical oceanographic observations to sedimentological analyses of the erosional and depositional bedforms. In this context, moorings were placed along the southern Adriatic basin and the location of the mooring sites was chosen on the basis of the most prospective passage of dense shelf water obtained through an integrated approach between modelling-based predictions and geology-driven inferences. From 2012 the monitoring was continued, leading to the collection of 8-years datasets of two sites placed in two different areas along the continental slope of the southern Adriatic Sea. The moorings are equipped with an acoustic Doppler current profiler (ADCP; Teledyne RD Instruments) system as well as conductivity, temperature and depth (CTD) probes that measure currents along the last 100 m of the water column and thermohaline properties. The moorings sites are in the western sector of the continental margin respectively at 700 and 600 m depth in an open furrow area of the continental slopes and in the main channel of the Bari Canyon System. The two different morphologies of the mooring site make the datasets representative of two different dynamic conditions of the continental slope of the southern basin.

This paper presents data collected from 2012 to 2020, of which short segments of the dataset relative to 2012 have been used in previous studies (Mihanovic et al., 2013; Chiggiato et al., 2016a, b; Langone et al., 2016; Marini et al., 2016; Foglini et al., 2016; Carniel et al., 2016; Bonaldo et al., 2016; Cantoni et al., 2016) for the analysis of physical processes (Chiggiato et al., 2016a) and particle dynamics (Langone et al., 2016) induced by the 2012 cascading events. The data collected from the moorings are part

Table 1. Survey details on the two mooring sites. Number of survey (no. 17), start and end of each survey, mooring position, depth of mooring site, and ADCP and CTD serial number (S/N) of instrument used.

	Mooring BB						Mooring FF					
No.	start	end	Mooring position (lat, long)	Depth (m)	ADCP S/N	CTD S/N	start	end	Mooring position (lat, long)	Depth (m)	ADCP S/N	CTD S/N
1	8 Mar 2012	21 Jun 2012	41°20.475′ N, 17°11.625′ E	504	1805	6134	8 Mar 2012	21 Jun 2012	41°48.364′ N, 17°02.292′ E	631	6422	1709
2	29 Jun 2012	6 Nov 2012	41°20.478′ N, 17°11.611′ E	504	1805	7041	30 Jun 2012	09 Nov 2012	41°48.373′ N, 17°02.292′ E	631	6422	7040
3	13 Dec 2012	18 Apr 2013	41°20.478′ N, 17°11.605′ E	504	6422	7040	9 Nov 2012	14 Apr 2013	41°48.367′ N, 17°02.296′ E	632	1805	7041
4	18 Apr 2013	8 Nov 2013	41°20.481′ N, 17°11.623′ E	504	1465	7041	15 Apr 2013	8 Nov 2013	41°48.360′ N, 17°02.292′ E	632	1805	7266
5	9 Nov 2013	9 Mar 2014	41°20.471′ N, 17°11.604′ E	504	17 316	7041	8 Nov 2013	9 Mar 2014	41°48.390′ N, 17°02.273′ E	632	17 315	7266
6	9 Mar 2014	1 Nov 2014	41°20.471′ N, 17°11.628′ E	504	17 316	7040	10 Mar 2014	2 Nov 2014	41°48.390′ N, 17°02.284′ E	632	17 315	7266
7	1 Nov 2014	20 Apr 2015	41°20.474′ N, 17°11.622′ E	500	17 316	7040	2 Nov 2014	22 Apr 2015	41°48.357′ N, 17°02.297′ E	632	17 315	7266
8	23 Apr 2015	9 Nov 2015	41°20.456′ N, 17°11.639′ E	500	17 315	7266	22 Apr 2015	6 Nov 2015	41°48.396′ N, 17°02.241′ E	636	17 316	7040
9	9 Nov 2015	1 Apr 2016	41°20.456′ N, 17°11.639′ E	503	17 316	7041	9 Nov 2015	2 Apr 2016	41°48.396′ N, 17°02.217′ E	632	17 315	7266
10	5 Apr 2016	23 Oct 2016	41°20.456′ N, 17°11.639′ E	497	17 316	6134	4 Apr 2016	23 Oct 2016	41°48.396′ N, 17°02.217′ E	632	17 315	7266
11	24 Oct 2016	23 Apr 2017	41°20.456′ N, 17°11.639′ E	497	17 316	6134	24 Oct 2016	23 Apr 2017	41°48.396′ N, 17°02.217′ E	632	17 315	7266
12	25 Apr 2017	2 Nov 2017	41°20.446′ N, 17°11.620′ E	497	17 316	7041	24 Apr 2017	2 Nov 2017	41°48.402′ N, 17°02.180′ E	632	17 315	7266
13	4 Nov 2017	9 May 2018	41°20.455′ N, 17°11.622′ E	497	17 316	7266	3 Nov 2017	9 May 2018	41°48.407′ N, 17°02.186′ E	632	17 315	7041
14	14 May 2018	7 Oct 2018	41°20.471′ N, 17°11.638′ E	496	17 315	6134	9 May 2018	9 Oct 2018	41°48.350′ N, 17°02.291′ E	632	17 316	7266
15	10 Oct 2018	25 Mar 2019	41°20.498′ N, 17°11.617′ E	500	17 316	7266	9 Oct 2018	24 Mar 2019	41°48.224′ N, 17°02.282′ E	632	17 315	6134
16	25 Mar 2019	19 Oct 2019	41°20.491′ N, 17°11.637′ E	498	17 316	7266	24 Mar 2019	20 Oct 2019	41°48.350′ N, 17°02.292′ E	632	6422	6134
17	20 Oct 2019	25 Jun 2020	41°20.518′ N, 17°11.645′ E	505	17 315	7266	20 Oct 2019	26 Jun 2020	41°48.316′ N, 17°02.351′ E	632	6422	6134

of the IFON network (Italian Fixed-Point Observatory Network, Ravaioli et al., 2016) and the southern Adriatic Sea observatory of the EMSO-Italy Joint Research Unit (http://emso.eu/observatories-node/south-adriatic-sea/ last access: 14 December 2022), and the continuous measurement activity provides a unique observatory on the hydrodynamic processes along the southern Adriatic slope that have a direct implication on water renewal and transfers of organic and inorganic particulate matter from the shelf to the deep sea.

2 Setting, instruments, data and methods

The data come from two moorings located along the continental slope of the southern Adriatic Sea (Fig. 1a). The mooring sites are placed in two different locations that differ from a geomorphological point of view. The mooring site called BB is placed at 600 m depth on the main branch of Bari Canyon System (BCS) at 41°20.456′ N, 17°11.639′ E, while the mooring site FF is placed at 41°48.396′ N, 17°02.217′ E on open slope furrow area of the continental slope at 700 m depth. The stand-alone moorings are equipped with an ADCP system which measures currents

along the last 100 m of the water column and a CTD probe located approximatively 10 m above the bottom. Moorings, still operative, were configured and maintained for continuous long-term monitoring following the approach of the CIESM Hydrochanges Program (https://www.ciesm.org/marine/programs/hydrochanges.htm last access: 07 December 2022; Schroeder et al., 2013). The 110 m long mooring scheme is represented in Fig. 1b. The ADCP system measures the intensity and directions of currents along the water column and has a temperature sensor in its transducer head. The CTD probe provides measurements of temperature and salinity (along with pressure). The measurements are extended from 2012 until 2020 and divided in separated deployments interspersed approximately every 6 months for instrumentation recovery, data downloading and maintenance.

The ADCP used is of the type RDI Workhorse (Teledyne RD Instruments USA, Poway, California), using a four-beam, convex configuration with a beam angle of 20° and a working frequency of 307 kHz. The instrument is moored at a mean nominal depth of 500 m (BB) and 600 m (FF) in downward-looking mode at roughly 100 m from the seabed. The number of depth cells is set to 27 with a cell size of 4 m. The sampling interval is set to 1800 s with 45 ping per ensemble. An ADCP computes sound speed based on an assumed salinity and transducer depth and on the temperature measured at the transducer. The system measures water temperature at the depth of the transducer by means of a thermistor embedded in the transducer head between the four beams. The sensor provides measurements in a range between −5–45 °C, with a precision of ± 0.4 °C and resolution of 0.01 °C.

Approximately at 10 m above the seabed, there is a CTD probe, SBE 16plus V2 SeaCAT to record thermohaline parameters. The SBE 16plus V2 SeaCAT is a high-accuracy CTD recorder designed for moorings or other long-duration, fixed-site deployments. In addition, the probe is equipped with optional pump for bio-fouling protection. Data of water conductivity were measured by sensor, with accuracy of 0.0005 S m^{-1} and resolution of 0.00005 S m^{-1}; the water temperature by means of a thermometer, with accuracy of 0.005 °C and resolution of 0.0001 °C; and the water pressure by means of a pressure strain gauge sensor, with an accuracy of 0.002 % of full-scale range.

The resulting dataset covers the period from 8 March 2012 to 26 June 2020 for both moorings (details about surveys are reported in Table 1 where there is the description about the temporal extensions of each measuring period, the mooring location, depth and S/N of the ADCP system used). The instrumentation recovery consists of data downloading, battery replacing and sensor checking together with maintenance operations. Every mooring component (ropes, chains and hooks) are checked to ensure the functionality, durability and resistance during the surveying period. The probes are cleaned from fouling and the sensor state is checked. Table 1 reports the S/N of instrumentation used in each deployment, which is useful to know when some probes were replaced. The probes were calibrated at Sea-Bird Europe – European Calibration and Repair Center – and Table 2 reports the date of calibration of each CTD probe. During the cruise of October 2018 and 2019 (detailed in the cruise report of Cardin et al., 2018 and Bubbi et al., 2019), comparison profiles are carried out with a calibrated onboard CTD probe, in order to ensure the measurement agreement. The onboard CTD is a SeaBird SBE 911plus equipped with dual sensors of temperature and conductivity. The pressure, temperature and conductivity sensors were calibrated at Sea-Bird Europe in September 2016. The CTD was attached to a SBE32 Carousel Water Sampler with 24 bottles (10 L) together with an altimeter. From three depth levels, depending on the vertical profile of the stations, water samples were also taken for calibration purposes of the salinity values, and they were analysed in the laboratory using a Guildline "Autosal" salinometer.

Table 2. Calibration date of the CTD probes named with the serial number (S/N).

CTD S/N	Calibration date
6134	September 2013–April 2014
7041	March 2012–February 2014
7040	March 2012–November 2016
7266	January 2013

The distances between the deployment points of the moorings during the different time period did not exceed 140 m for BB and 306 m for FF.

The ADCP time series is not fully continuous, not for instrument failures but for operational reasons linked to recovering and sailing during maintenance surveys. Interruptions occurred twice a year, approximately every 6 months (at the end of winter and in autumn), trying to make them as short as possible. The CTD time series follows the deployment of ADCP but sampling strategy is not always in agreement with ADCP time series and the continuity of the dataset.

The sampling interval in the BB site was always at 1800 s and continuity of the data reflected those of ADCP records, except for a data gap due to battery discharge, that extended from 31 July to 9 November 2015. In the FF site, the sampling interval in the first survey was 600 s; in the 5th, 9th, 10th and 11th surveys, the sampling interval was 3600; and in the 7th survey, the sampling interval was 10 800 s. The continuity of the data reflects those of ADCP records, except for two data gaps, due to malfunctioning and battery discharge, that extended from 14 August 2013 to 8 November 2013 and from 30 May 2014 to 2 November 2014.

2.1 Dataset and metadata description

The dataset is composed of four files in NetCDF format containing observational data and related metadata from the two mooring sites (BB and FF) for the period March 2012–

Table 3. The qualifier flag codes relevant to this work are given in the table. The full list is available at the following address: http://seadatanet.maris2.nl/v_bodc_vocab_v2/browse.asp?order=conceptid&formname=search&screen=0&lib=l20, last access: 7 December 2022.

Key	Entry term	Term definition
0	No quality control	No quality control procedure has been applied
1	good	Good quality data value. Verified as consistent during quality control process
2	Probably good value	Data value probably consistent, but this is unconfirmed
3	Probably bad value	Data value recognised as inconsistent after quality control
4	Bad value	An obviously erroneous data value
5	Changed value	Data value changed after quality control
6	Value below detection	The level of the measured phenomenon was too small to be quantified by the technique employed to measure it
7	Value in excess	The level of the measured phenomenon was too large to be quantified by the technique employed to measure it
8	Interpolated value	This value has been derived by interpolation from other values in the data object
9	Missing value	The data value is missing

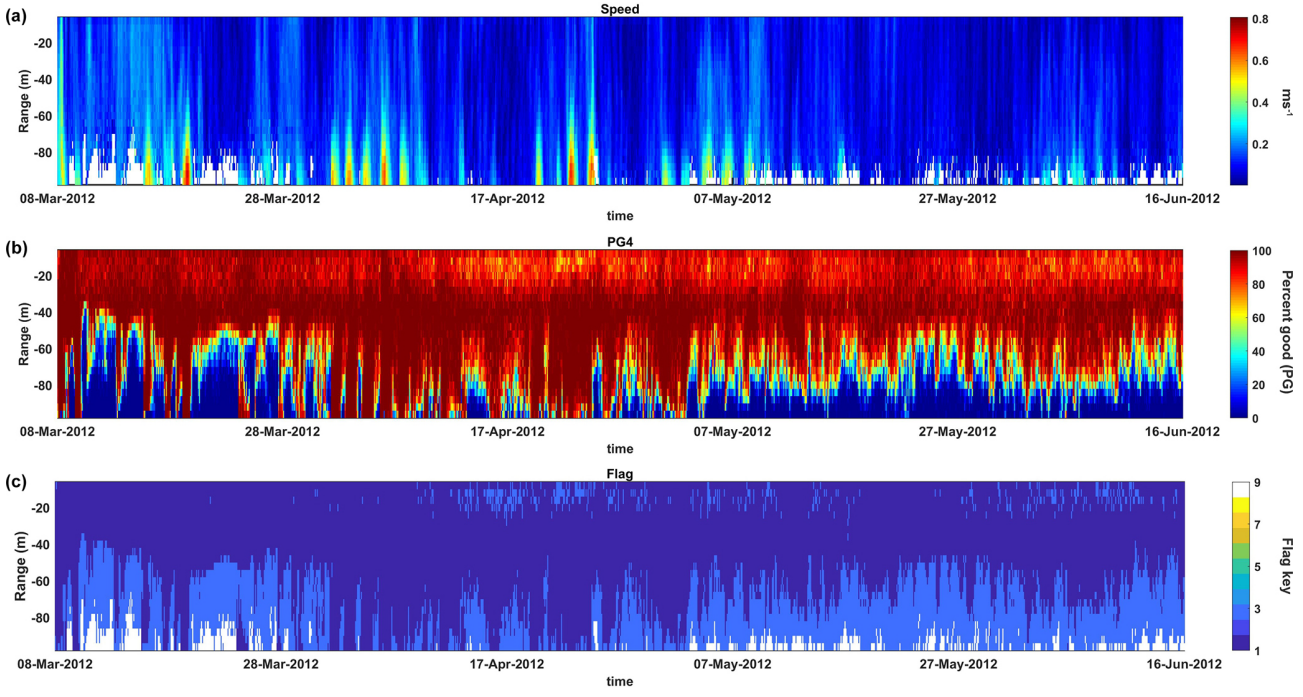

Figure 2. Schematic of the quality control procedure: in **(a)**, the original current velocity data are represented, in **(b)**, the value of the percent good parameter calculated for each cell is represented, and in **(c)**, the key of the qualifier flag assigned for each observation is represented. For better visualisation, only part of the time series has been represented.

June 2020. Each mooring site has two datasets for ADCP and CTD data, respectively, and each filename specifies the mooring site name, its depth and the instrument (ADCP or CTD).

The data and metadata information includes global attributes, dimensions and variables. Global attributes contain a summary description of the dataset and details about their geospatial position, temporal extension and data interval, the institution responsible of measurements, principal investigator's name and contact, the observational network to which the mooring belongs, the conventions ("OceanSITES v1.4,SeaDataNet_1.0,COARDS,CF-1.6") and keywords vocabulary ("SeaDataNet parameter discovery vocabulary") used. Dimensions have the available structure of variables. For each variable, the following is reported: the size, the dimensions, the data type and attributes which last give specific information about each variable, such as the measured parameter, the unit, the sensor, the data value range, etc.

Regarding the ADCP dataset, it provides details about the station name, the probe serial numbers, the geographical po-

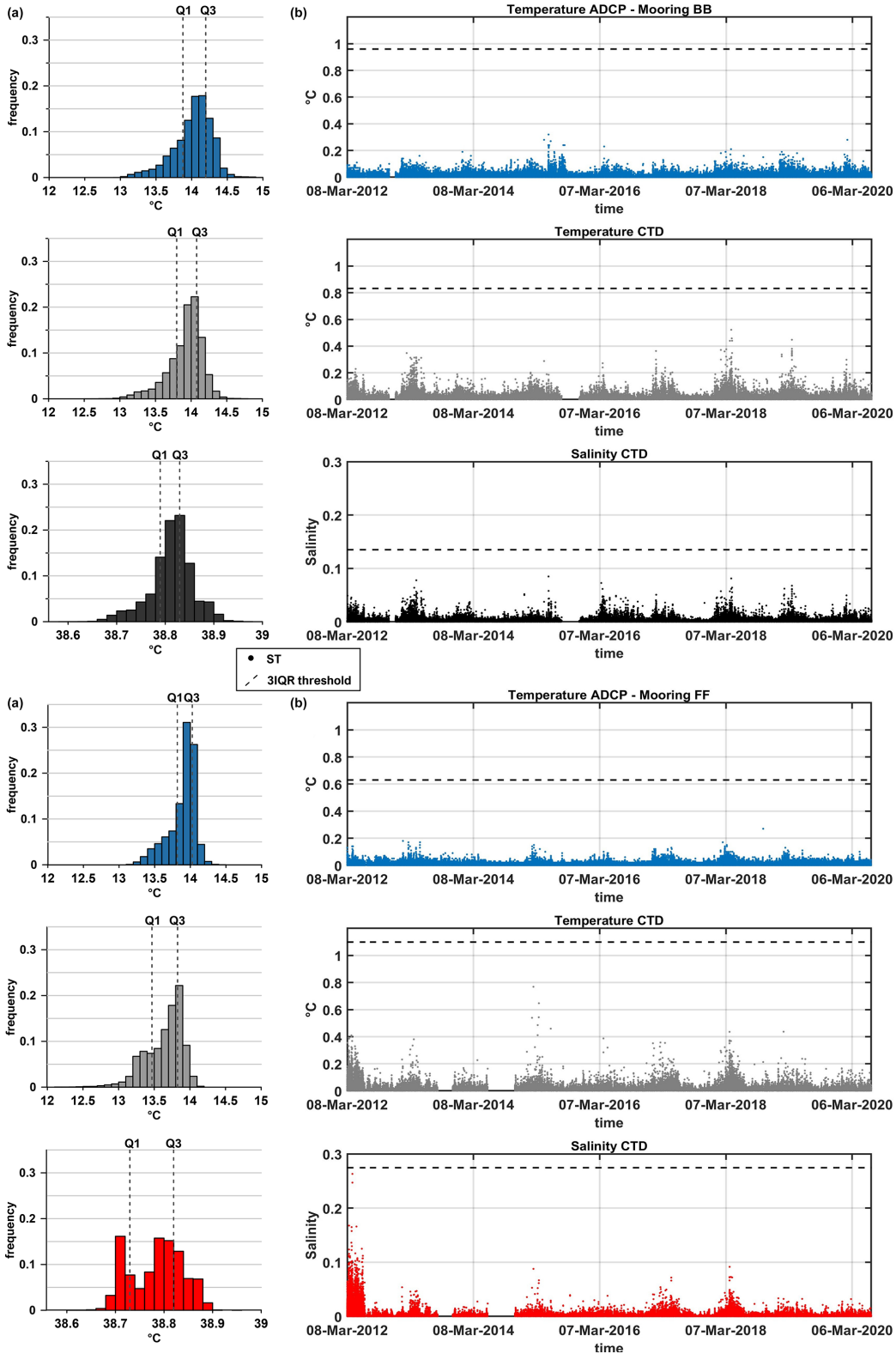

Figure 3. Quality control of temperature and salinity data measured by ADCP and CTD. **(a)** The distributions of the temperature and salinity data recorded at each berth are shown, and Q1 and Q3 represent the 25th and 75th percentiles used for IQR calculation. **(b)** The time series of the ST value calculated for each observation (dots) and the 3IQR value (dashed line) indicating the threshold for identifying outliers are shown.

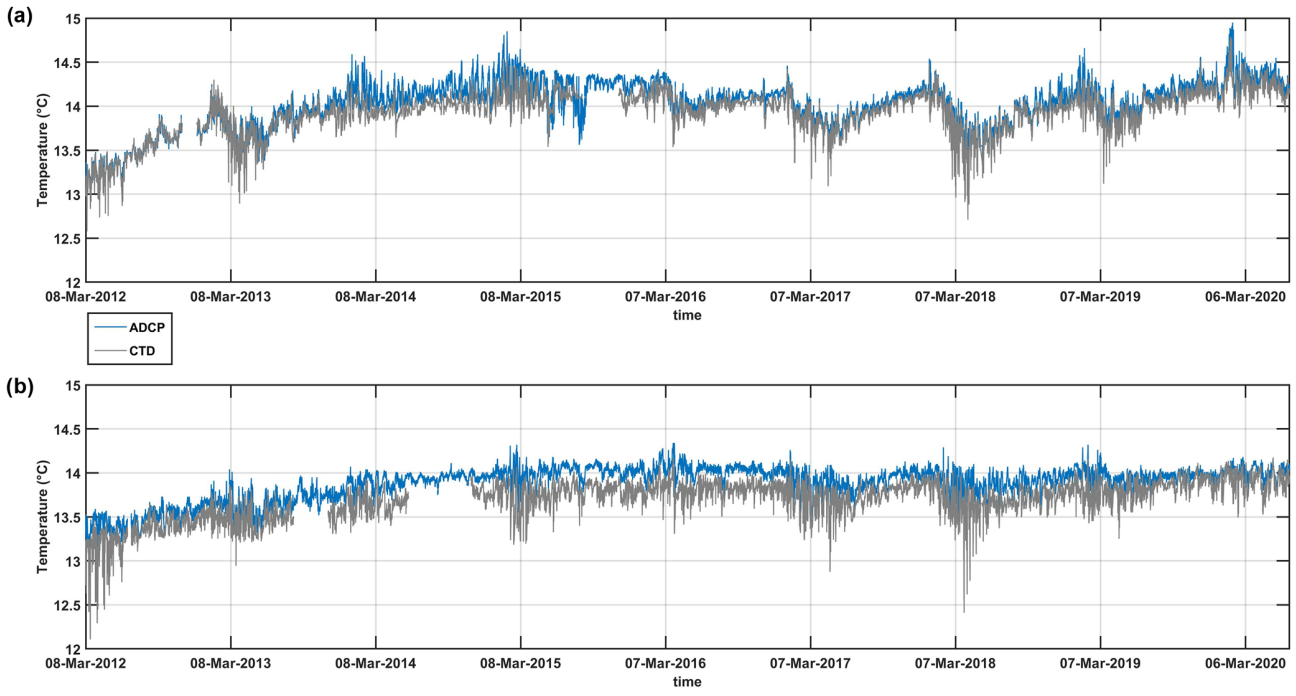

Figure 4. ADCP and CTD temperature records at two mooring sites, **(a)** BB on canyon (600 m depth) and **(b)** FF on the open slope (700 m).

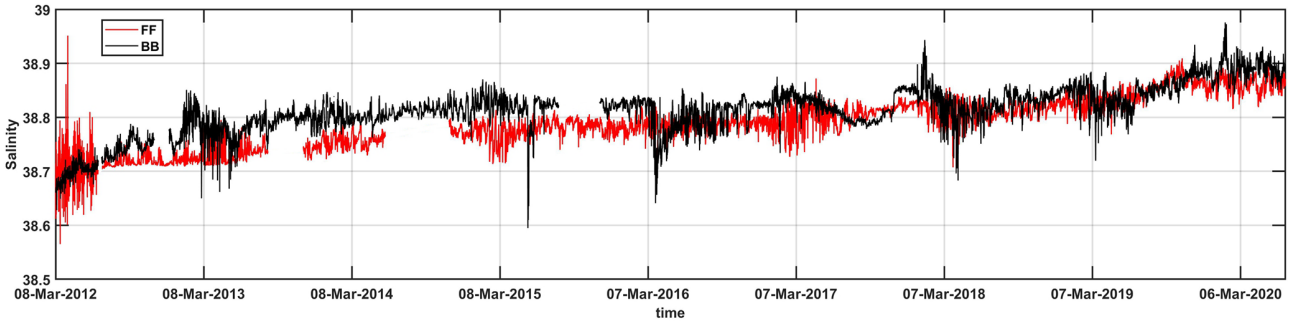

Figure 5. CTD Salinity records on the two mooring sites BB and FF.

sition, the time, the depth, the cell depth and the component east, north and vertical of the current speed. The dataset contains the original ADCP variables followed by the qualification flags according to the results of the quality control (QC) procedure described in the next chapter. Regarding CTD, it reports the original data and qualifier flags, which define the quality of temperature and salinity data. The headers of the quality flag assigned for each variable are followed by the suffix "-_qc".

It is ensured that all data described here are findable, accessible, interoperable and reusable (according to the FAIR principles, Tanhua et al., 2019), since they are identified by a unique persistent identifier (see abstract and Data Availability section). This also allows them to be retrievable, with all metadata records being accessible as well. Permanent DOI and metadata ensure findability of the dataset. The permanent accessibility of the dataset is allowed by the use of Zenodo public repository. The data are available in NetCDF format, which ensures the Interoperability with other platforms. The data and metadata specified in the global attributes use the SeaDataNet parameter discovery vocabulary (https://www.seadatanet.org/Standards/Common-Vocabularies, last access: 7 December 2022) and the conventions OceanSITES v1.4,SeaDataNet_1.0,COARDS,CF-155 1.6. The metadata accurately describe the data, ensuring their reusability in future research and their integration with other data sources.

2.2 Data quality check

A first visual check of ADCP and CTD data time series gives a quick idea about whether the data look reasonable or not, judging by the average values of the parameter measured and the overall "noisiness" of the plot. This screening phase al-

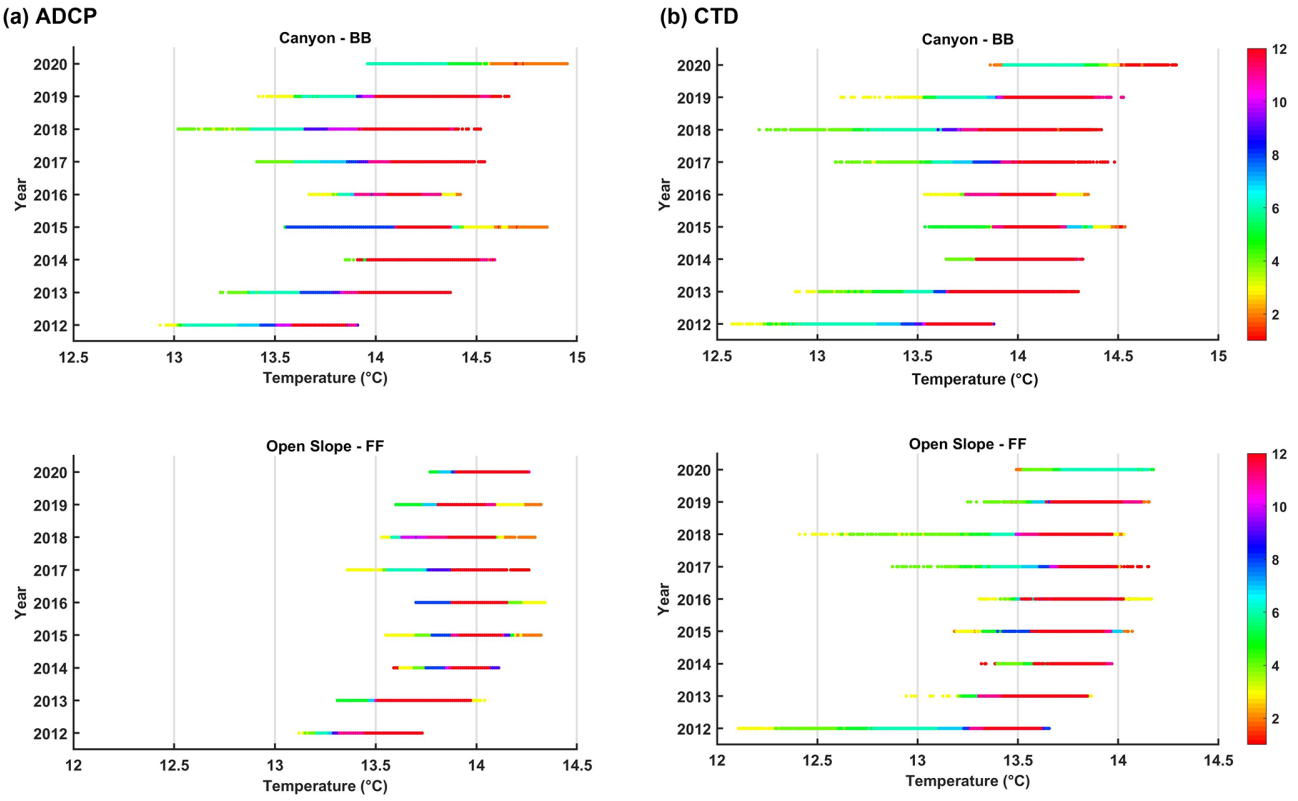

Figure 6. Scatterplot of ADCP **(a)** and CTD **(b)** temperature grouped by years (y axis) and months (colour scale).

lows to detect anomalous values, which are those out of range with the rest of the series, and helps to exclude from the time series data when systems are outside the water, determining the corrected start and end of the time series. One parameter that helps this first screening phase is the depth measured by the pressure sensor, which indicates when the probe is at the operating depth and when it is being recovered at the surface. Applying these checks, a maximum of 1.95 % of data of BB and 1.48 % of data of FF were removed from the dataset.

Regarding ADCP data, a second step consists of the determination of the seabed and the portion of the water column with good data. The seabed is detected by a specified filter algorithm named "side lobe interference", which is based on the principle that the echo through the side lobe facing the surface or the bottom returns to the ADCP at the same time as the echo from the main lobe at certain distance to the surface that depends on the beam angle. In the case of a beam with an angle of 20°, this means data from the last 6 % of the range to the bottom can be contaminated. When looking down, as in our case, the contamination from bottom echoes usually biases velocity data toward zero. The next data processing applies a data QC criterion based on the parameter "percentage good", provided from the recording system, and indicates the fraction of data that passed a variety of criteria which include low correlation, large error velocity and fish detection (false target threshold). To ensure the robustness of the collected data, we have used a threshold of 80 % to define good data (PG80). The structure of the data matrix explained in the published database metadata consists of the original data, to ensure data accessibility and reusability, and a quality flag is assigned to each observation following the SeaDataNet QC guidelines (SeaDataNet, 2010) and the L20 SeaDataNet Measurand Qualifier flags (last updated at http://seadatanet.maris2.nl/v_bodc_vocab_v2/browse.asp?order=conceptid&formname=search&screen=0&lib=l20), as shown in Table 3.

As shown in Fig. 2 where an example of quality control procedure is depicted, when the hydrodynamic data exceed the PG80 threshold, the quality flag assigned corresponds to code 3 which indicates the value recognised as inconsistent after QC, while when the data pass the QC, the assigned flag is 1. Flag 9 is assigned when data are missing in the original time series.

For CTD measurements, the raw hexadecimal data were converted to ASCII by the SBE Data Processing™, and after visual inspection, QC tests were applied to the data according to SeaDataNet guidelines (SeaDataNet, 2010), which rely on a spike (ST) and a gradient test (GT):

The ST evaluates if the differences between sequential measurements are too large ($ST > 6\,°C$ for temperature, $ST > 0.9$ for salinity), as follows:

$$ST = |V_2 - (V_3 + V_1)/2| - |(V_3 - V_1)/2|,$$

Table 4. Statistical parameters of temperature records of the two moorings grouped by months. SD indicates standard deviation and Δ is the mean difference between temperature measured by ADCP and CTD and Δ_{max} is the maximum difference. The values reported in the table refer to original data (not smoothed).

MOORING BB										
Month	Mean (°C)		SD		Min (°C)		Max (°C)		Δ (°C)	Δ_{max} (°C)
	ADCP	CTD	ADCP	CTD	ADCP	CTD	ADCP	CTD		
1	14.20	14.07	0.20	0.17	13.69	13.35	14.89	14.79	0.13	0.60
2	14.15	14.02	0.22	0.18	13.38	13.17	14.95	14.62	0.13	0.73
3	13.95	13.83	0.34	0.33	12.93	12.58	14.65	14.50	0.11	0.53
4	13.88	13.79	0.34	0.33	13.02	12.71	14.51	14.44	0.10	0.66
5	13.89	13.8	0.31	0.28	13.03	12.75	14.55	14.4	0.09	0.61
6	13.93	13.86	0.28	0.26	13.05	12.87	14.41	14.37	0.07	0.34
7	13.95	13.89	0.24	0.21	13.32	13.3	14.37	14.31	0.06	0.29
8	13.98	13.90	0.20	0.17	13.43	13.42	14.36	14.17	0.06	0.52
9	14.06	13.95	0.20	0.14	13.51	13.49	14.41	14.25	0.08	0.37
10	14.06	13.97	0.20	0.16	13.51	13.53	14.52	14.26	0.06	0.46
11	14.16	14.04	0.14	0.12	13.69	13.65	14.59	14.53	0.12	0.49
12	14.13	14.03	0.16	0.14	13.59	13.55	14.54	14.48	0.11	0.41
MOORING FF										
Month	Mean (°C)		SD		Min (°C)		Max (°C)		Δ (°C)	Δ_{max} (°C)
	ADCP	CTD	ADCP	CTD	ADCP	CTD	ADCP	CTD		
1	13.97	13.76	0.14	0.14	13.50	13.25	14.29	14.15	0.19	0.63
2	13.95	13.71	0.16	0.16	13.51	13.18	14.49	14.15	0.21	0.93
3	13.86	13.53	0.23	0.23	13.12	12.11	14.34	14.17	0.22	1.23
4	13.85	13.50	0.20	0.20	13.15	12.29	14.22	14.08	0.22	1.19
5	13.82	13.53	0.23	0.23	13.22	12.61	14.18	14.18	0.18	0.77
6	13.88	13.60	0.20	0.20	13.21	12.76	14.15	14.15	0.18	0.54
7	13.86	13.66	0.20	0.20	13.27	13.11	14.17	14.02	0.16	0.51
8	13.89	13.70	0.17	0.17	13.41	13.23	14.18	14.01	0.16	0.57
9	13.91	13.72	0.18	0.18	13.29	13.26	14.17	14.05	0.17	0.44
10	13.92	13.74	0.17	0.17	13.36	13.27	14.21	14.05	0.17	0.51
11	13.92	13.74	0.17	0.17	13.32	13.26	14.26	14.11	0.16	0.49
12	13.93	13.75	0.16	0.16	13.45	13.33	14.25	14.03	0.16	0.54

where V_2 is the measurement being tested as a spike and V_1 and V_3 are the previous and next values.

The GT evaluates if the gradient between adjacent salinity and temperature measurements are too steep (GT < 9 °C for temperature, GT > 1.5 for salinity), as follows:

$$\mathrm{GT} = |V_2 - (V_3 + V_1)/2|,$$

where V_2 is the measurement being tested and V_1 and V_3 are the previous and next values.

The threshold considered in the spike test of the SeaDataNet procedure is a fixed value and extremely large when considering the variability of our data. Therefore, the quality control of temperature and salinity was implemented by defining an appropriate threshold for the data based on statistical analysis. The threshold was obtained from the calculation of the IQR parameter (Hald, 1952), which is a parameter used in the identification of outliers in non-symmetrically distributed data. The IQR parameter is estimated from the 25th (Q1) and 75th (Q3) percentiles through the relationship, IQR = Q3 − Q1, from which the threshold for identifying an outlier is obtained, which is equal to 3 × IQR (3IQR). For each mooring, both the distributions of temperature and salinity data with the values corresponding to Q1 and Q3 are shown (Fig. 3a), as well as graphs of the ST values calculated for each dataset with the 3IQR quality control threshold reference (Fig. 3b).

When QC computation is completed, the time series is organised with every observation followed by specific flag code according to the SeaDataNet qualifier flag: data that pass the QC test are flagged with code 1 and data that do not pass the test are flagged with code 4.

Applying these guidelines, no anomalies and spikes were found in the dataset. In the dataset, all data are reported ex-

Table 5. Statistical parameters of temperature records of the two moorings grouped by years. SD indicates standard deviation and Δ is the mean difference between temperature measured by ADCP and CTD and Δ_{max} is the maximum difference. The values reported in the table refer to original data (not smoothed).

MOORING BB										
Month	Mean (°C)		SD		Min (°C)		Max (°C)		Δ (°C)	Δ_{max} (°C)
	ADCP	CTD	ADCP	CTD	ADCP	CTD	ADCP	CTD		
2012	13.47	13.46	0.19	0.22	12.93	12.58	13.91	13.88	0.02	0.45
2013	13.87	13.79	0.17	0.18	13.23	13.89	14.37	14.30	0.07	0.61
2014	14.16	13.99	0.11	0.09	13.85	13.64	14.59	14.32	0.17	0.56
2015	14.25	14.10	0.17	0.12	13.55	13.54	14.85	14.53	0.16	0.57
2016	14.11	14.04	0.12	0.11	13.67	13.54	14.42	14.35	0.08	0.46
2017	13.98	13.92	0.16	0.16	13.41	13.09	14.54	14.48	0.07	0.50
2018	13.91	13.83	0.21	0.22	13.02	12.71	14.52	14.42	0.08	0.66
2019	14.10	14.01	0.16	0.16	13.42	13.12	14.66	14.53	0.09	0.56
2020	14.33	14.22	0.15	0.12	13.96	13.86	14.95	14.79	0.11	0.73
MOORING FF										
Month	Mean (°C)		SD		Min (°C)		Max (°C)		Δ (°C)	Δ_{max} (°C)
	ADCP	CTD	ADCP	CTD	ADCP	CTD	ADCP	CTD		
2012	13.48	13.26	0.11	0.19	13.12	12.11	13.73	13.66	0.16	1.23
2013	13.68	13.48	0.12	0.12	13.31	12.94	14.04	13.87	0.17	0.64
2014	13.93	13.67	0.07	0.11	13.59	13.32	14.11	13.97	0.23	0.63
2015	14.01	13.79	0.08	0.10	13.55	13.18	14.32	14.07	0.24	0.93
2016	14.04	13.82	0.08	0.09	13.70	13.31	14.34	14.17	0.22	1.01
2017	13.91	13.74	0.10	0.13	13.36	12.88	14.26	14.15	0.17	1.05
2018	13.90	13.69	0.10	0.15	13.53	12.41	14.29	14.03	0.21	1.23
2019	14.96	13.82	0.08	0.12	13.60	13.25	14.32	14.15	0.14	0.69
2020	14.05	13.91	0.08	0.12	13.77	13.49	14.26	14.18	0.11	0.47

cept when the probe is outside the water and not at the correct mooring depth. The flag 9 is assigned when data are missing.

3 Results

3.1 Thermohaline records

Temperature is measured by ADCP and CTD at two different depths along the water column, respectively, at roughly 100 m above the bottom (m a.b.) and 10 m a.b. The time series shown in Fig. 4 in both sites starts in March 2012 after the cold air outbreak occurred in the northern Adriatic, and the time series starts during cascading events well known in literature (Chiggiato et al., 2016b).

In the upper layer (100 m a.b.), the temperature recorded by ADCP in the BB site has a mean value of 14.02 ± 0.27 °C with a minimum temperature of 12.93 °C and maximum of 14.95 °C. In the lower layer (10 m a.b.), the CTD highlighted an average temperature of 13.92 ± 0.24 with a minimum temperature of 12.57 °C and maximum of 14.78 °C.

In FF at 100 m a.b., the mean recorded temperature is 13.89 ± 0.19 °C with a minimum temperature of 13.12 °C and maximum of 14.49 °C, while near the bottom (10 m a.b.), the measurements indicate average value of 13.64 ± 0.26 °C with a minimum temperature of 12.10 °C and maximum of 14.17 °C.

Observing the total time series of Fig. 4, the two sites have synchronous fluctuations more marked in the BB site. In addition, in the BB site, the temperature's slight differences can be appreciated between the two measurements depth, while in the FF site, the temperature closest to the bottom is generally lower and has more pronounced variations. The time series shows a periodicity of water cooling with an almost constant annual frequency, but variable between years. The most marked events besides 2012 are 2013, 2017 and 2018.

Regarding salinity measurements in the BB site, in the lower layer, the average salinity is about 38.81 ± 0.04 (minimum of about 38.59 and maximum 38.97). In the FF site, the salinity records at 10 m a.b. have a mean value of 38.78 ± 0.05 PSU (minimum of about 38.64 PSU and maximum of 38.95 PSU).

The total time series of salinity in Fig. 5 has more marked variations in the BB site where the salinity is generally higher than the FF site. From 2018, a positive trend is appreciable in both sites and less differences between sites occur.

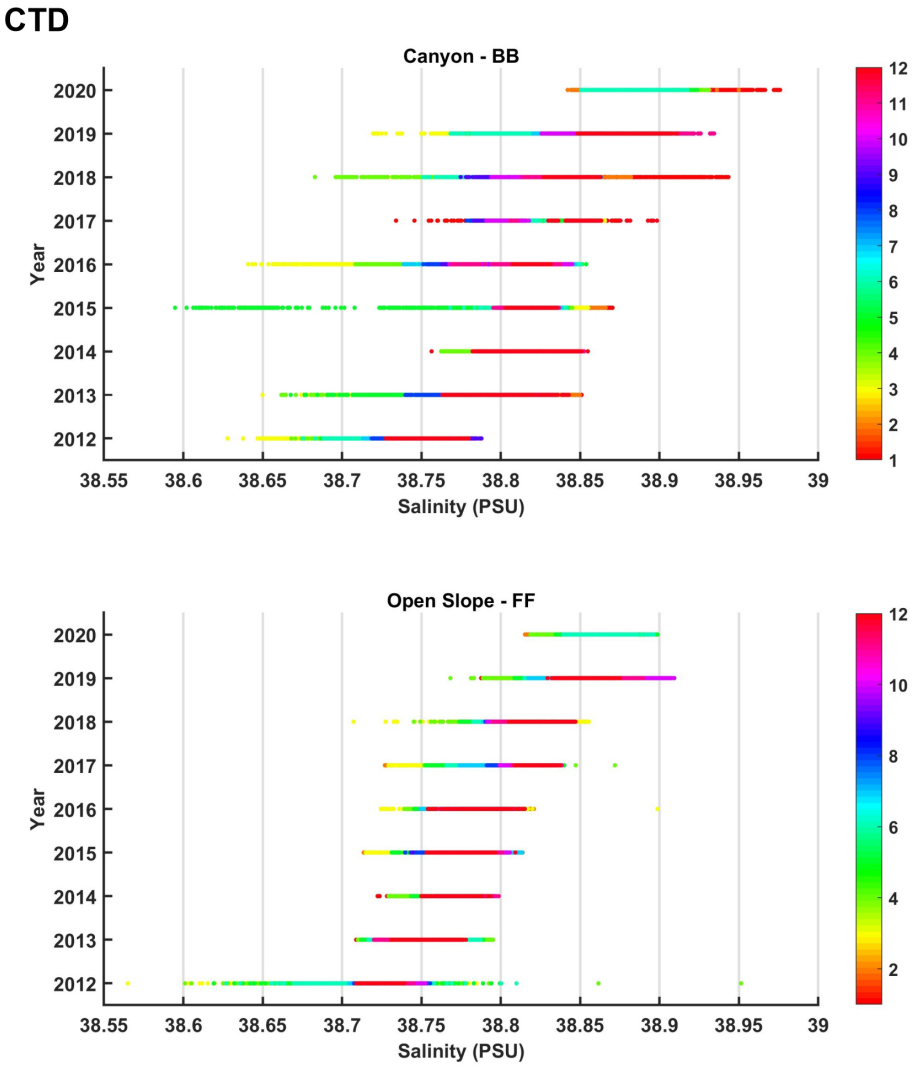

Figure 7. Scatterplot of salinity records grouped by years (y axis) and months (colour scale).

The temperature data in Fig. 6a are represented to give a quick overview of the inter- and intra-annual variability of the data. In the scatterplot, the temperature is distributed along the x axis and separates different months by colours. In the upper layer of the FF site, the variations are restricted in a narrow range, while in the lower layer, wide temperature fluctuations are visible and always concentrated between February and June. In BB, the vertical variability is less marked, but the time window when temperature decreases coincides. Statistics about temperature records grouped by months and years are reported in Tables 4 and 5, analysing mean and maximum differences between upper (ADCP) and lower (CTD) layers. Generally, the temperature differences between ADCP and CTD layer is constrained around 0.05 and 0.2 °C in both sites, and experience from January to May the largest decrease of water temperature especially close to the seabed. While in BB the maximum temperature difference between the upper and lower layer is 0.73 °C, in FF this can exceed 1 °C. The most intense cooling of water occurs in both sites during 2012, 2013, 2017 and 2018 when vertical difference increases. During 2019, only in the BB site, cool events occur with less intensity than the others. On an annual scale, large vertical temperature differences occur in FF, while in BB the difference is less evident.

Salinity data are represented in Fig. 7 in the same way as temperature. In this case, observations are limited only to the layer close to the seabed where the CTD probe is moored. In the FF sites, the variations are restricted in a narrow range, except during 2012, but in both sites the salinity decrease is always concentrated between February and June. Statistics about salinity records grouped by months and years are reported in Table 6. Generally, the variation of mean salinity between months is very narrow (< 0.02) in both sites, but between February and June salinity has got the maximum de-

Table 6. Statistical parameters of salinity records of the two moorings grouped by months and years. SD indicates standard deviation and Δ is the mean difference between temperature measured by ADCP and CTD and Δ_{max} is the maximum difference. The values reported in the table refer to original data (not smoothed).

Month	MOORING BB				MOORING FF			
	Mean	SD	Min	Max	Mean	SD	Min	Max
1	38.84	0.04	38.73	38.98	38.80	0.05	38.71	38.89
2	38.84	0.03	38.75	38.95	38.80	0.05	38.71	38.89
3	38.81	0.06	38.63	38.93	38.77	0.06	38.57	38.90
4	38.80	0.06	38.66	38.93	38.77	0.06	38.60	38.95
5	38.80	0.05	38.60	38.92	38.77	0.06	38.62	38.90
6	38.81	0.04	38.68	38.92	38.78	0.05	38.63	38.90
7	38.80	0.03	38.71	38.87	38.78	0.04	38.64	38.86
8	38.80	0.04	38.72	38.87	38.79	0.04	38.71	38.87
9	38.81	0.03	38.74	38.89	38.80	0.05	38.71	38.90
10	38.81	0.03	38.73	38.89	38.80	0.05	38.71	38.91
11	38.83	0.03	38.75	38.93	38.80	0.05	38.71	38.89
12	38.83	004	38.73	38.91	38.80	0.05	38.71	38.89
Year	Mean	SD	Min	Max	Mean	SD	Min	Max
2012	38.73	0.03	38.63	38.79	38.71	0.01	38.57	38.95
2013	38.79	0.02	38.65	38.85	38.73	0.02	38.71	38.80
2014	38.81	0.01	38.76	38.86	38.76	0.01	38.72	38.80
2015	38.82	0.03	38.60	38.87	38.78	0.01	38.71	38.81
2016	38.80	0.03	38.64	38.85	38.79	0.01	38.72	38.90
2017	38.82	0.02	38.73	38.90	38.81	0.02	38.73	38.87
2018	38.83	0.02	38.68	38.94	38.81	0.01	38.71	38.86
2019	38.85	0.03	38.72	38.93	38.85	0.03	38.64	38.91
2020	38.89	0.02	38.84	38.98	38.86	0.01	38.82	38.90

crease of more than 0.1. On an annual scale, the largest variations occur in both sites during 2012, 2013, 2017 and 2018. In the BB site, high variability of salinity is also observed in 2015 and 2016.

3.2 Hydrodynamic records

In this section, we present the hydrodynamic measurements along the water section measured by the ADCP from 2012 to 2020 in BB site and in the FF site. In order to detail the dynamic variability along the water column, the water column is separated in the three vertical layers (roughly to one-third of the measured water column): upper layer (UL), intermediate layer (IL) and lower layer (LL). In the polar histogram, the directions are binned every 5° and speed is divided in three classes.

BB site

Figure 8 shows the 8-years-long ADCP records at the BB site as vertical distribution of the speed module along the 23 layers of the water column (Fig. 8a), as polar histograms (Fig. 8b) and as polar scatterplots (Fig. 8c) which represent the direction and intensity of currents along the water column. Generally, the current field is very weak ($0.07 \pm 0.01\,m\,s^{-1}$), but during episodic energetic events the flow may exceed $0.5\,m\,s^{-1}$. The polar histograms represent hydrodynamic climate (Fig. 8b) where speed and directional class are clustered to represent the occurrence probability of the events, while in Fig. 8c it is possible to observe the magnitude and direction of every single event scattered on a polar diagram. The hydrodynamic field of the three layers highlights currents which spread between 100–225° N with a reigning directional sector in the upper layer between 170 and 200° N. The directional spreading of currents assumes a clear bimodal behaviour approaching toward the seabed with reigning currents SSW-oriented and dominant currents oriented toward SE. This behaviour is more marked at the bottom and indicates a flow oriented toward the canyon axis to 110° or southward along the direction of the isobath (Chiggiato et al., 2016a). This is a robust feature of this location (Turchetto et al., 2007) where currents directed along-canyon are directly associated to cascading flow while southward flow is indirectly associated to cascading as geostrophically adjusted downslope flow (Chiggiato et al., 2016a). The diagrams Fig. 8b and c of the LL clearly explain the dynamics of along-canyon axis currents which dominate in terms of intensity despite their low contribution in terms of frequency.

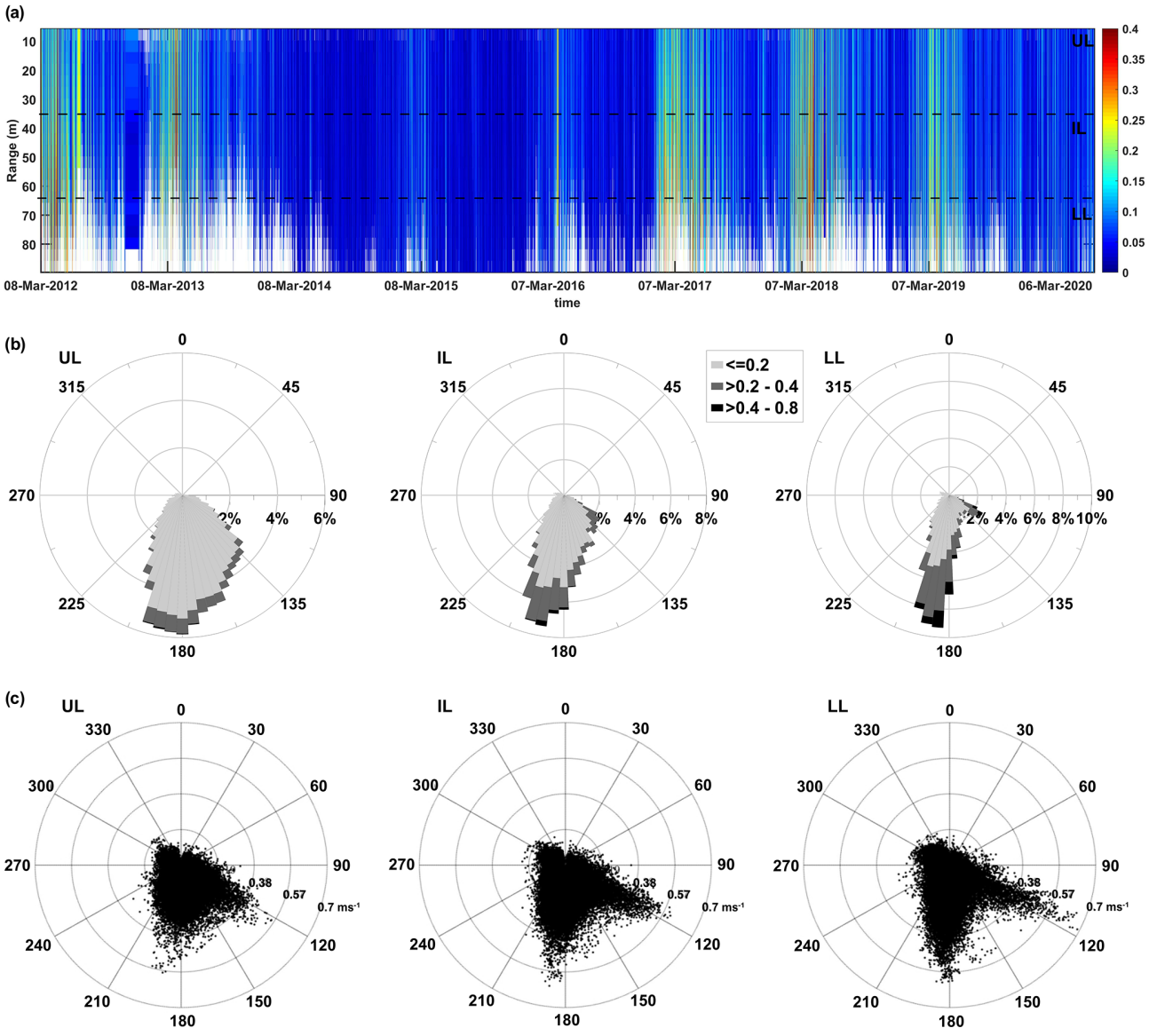

Figure 8. **(a)** Currents' speed records along the water column (data represented are filtered by 80 % percent good), dotted box indicates the water column corresponding to the three layers used for polar plot representation. **(b)** Polar probability plot of current velocity in the three layers of the water column ($m\,s^{-1}$). **(c)** Polar scatterplot of observed directional current velocity ($m\,s^{-1}$) (UL: upper layer; IL: intermediate layer; LL: lower layer) – BB.

Figure 9 shows the time series of the currents of the UL and LL represented with a "moving average" 7-daily smoothing which allows a better visualisation of the data by highlighting the vertical variability of currents especially during periods of flow intensification.The average speed of the currents is $0.069 \pm 0.005\,m\,s^{-1}$ in the UL and 0.079 ± 0.006 in the LL, and the flow accelerations when they occur involve the entire observed water column reaching a maximum speed of $0.76\,m\,s^{-1}$ in the LL and $0.58\,m\,s^{-1}$ in the UL. The maximum difference between UL and LL reaches a maximum value of $0.38\,m\,s^{-1}$.

An acceleration of the flow occurs approximately every year between February and May. The intensification of the current field varies year by year and reaches the greatest magnitude in 2012 and 2018 on the contrary of the weakest during 2014 and 2015. During energetic events, a general increase of the current speed toward the seabed is visible and the components of flows have positive values for the east component and negative for the northern. The vertical component has small values in a range of -0.01–$0.05\,m\,s^{-1}$ and is mainly directed toward the bottom during current pulses. The behaviour of components reflects the direction of flow

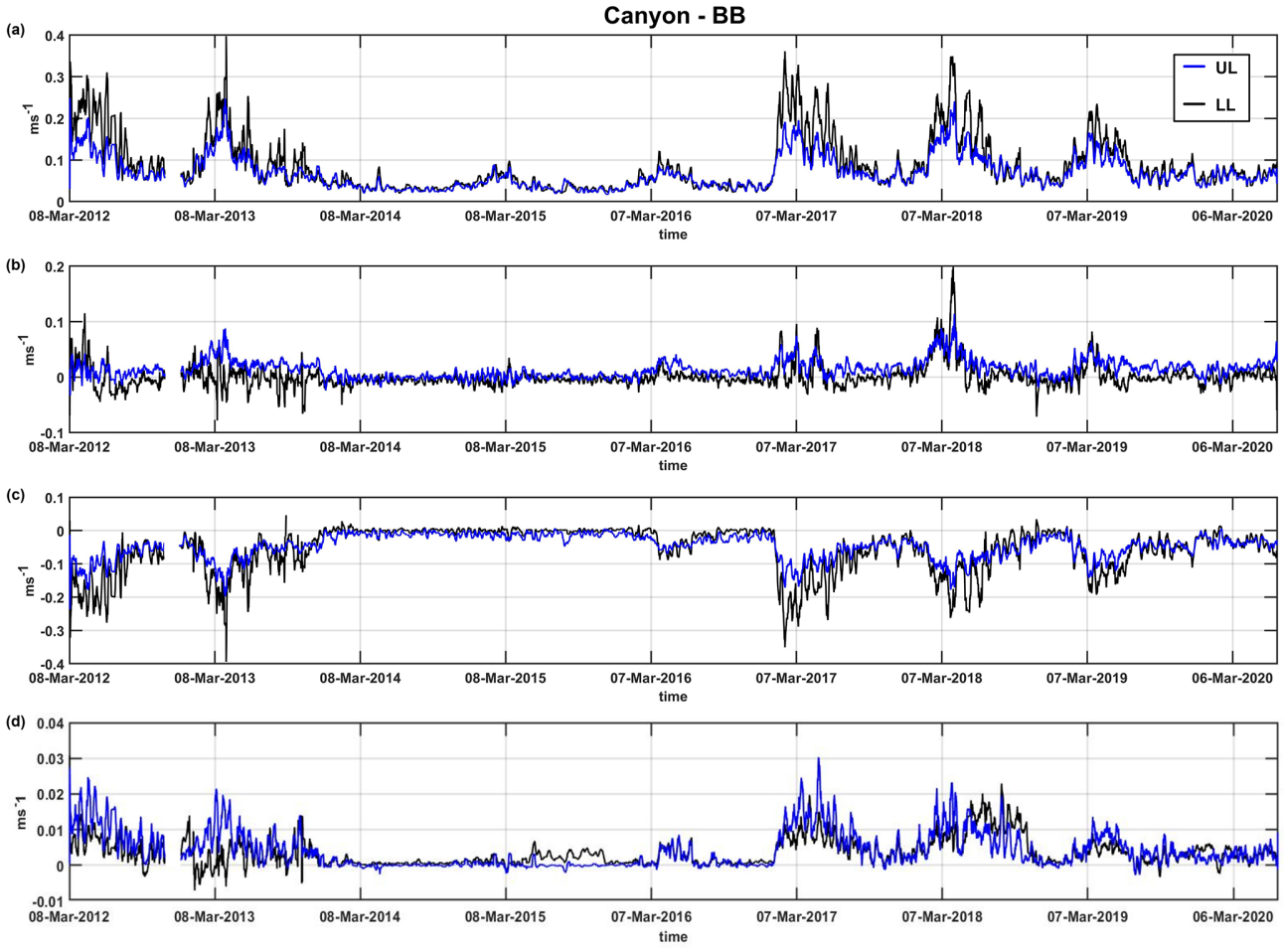

Figure 9. Time series of currents at BB site in the upper (UL) and lower layer (LL) of the water column: **(a)** speed, **(b)** east, **(c)** north and **(d)** vertical component – BB. The data are presented with a 7 d smoothing window.

appreciable in the polar plots (Fig. 8c) which are directed mainly toward S and SE.

FF Site

In the site FF, the 8-years records show an average weak hydrodynamic field with value of $0.05 \pm 0.01\,\mathrm{m\,s^{-1}}$ able to reach speed until $0.79\,\mathrm{m\,s^{-1}}$ during the episodic strong current pulses (Fig. 10a). As observed in the BB site, the pulses of currents in FF recur in a temporal window every year (between February and May). The three layers represented in the polar histogram plots of Fig. 10b (constructed in the same way of BB) details the vertical variability of the flow along the water column. The flow in the UL is southward within a directional range centred to 180° N, with more than 99 % of the datasets below the intensity of $0.2\,\mathrm{m\,s^{-1}}$. Proceeding down in the IL, the directional spreading of currents becomes narrow (always centred to 180° N) and the intensity slightly increases, remaining always below $0.4\,\mathrm{m\,s^{-1}}$. In the LL, intense currents are clearly visible (magnitude greater than $0.6\,\mathrm{m\,s^{-1}}$) directed toward south-east (150° N) in addition to the contour-parallel background current regime directed southwards. These intense events, with a very scarce frequency, indicate ageostrophic dynamics determined by the steepness of the continental margin which allows to break the geostrophic constraints (Chiggiato et al., 2016a) flowing downward on open slopes responsible for the origin of furrow marks reported in this site by Trincardi et al. (2007a). In the time series of the upper and lower layers, the currents' speed (Fig. 11) has an average value very similar, $0.049 \pm 0.003\,\mathrm{m\,s^{-1}}$ (UL) and $0.057 \pm 0.012\,\mathrm{m\,s^{-1}}$ (LL), but during pulses the speed increase concentrates at the bottom. During these events, the velocity difference between LL and UL can reach $0.51\,\mathrm{m\,s^{-1}}$.

During the acceleration phases of currents, the components of flow have a positive increment of eastern component together with a greater negative acceleration of the northern component. The eastern component in the UL never increases sensibly, while near the seabed it has the greatest increment. The vertical component is very weak

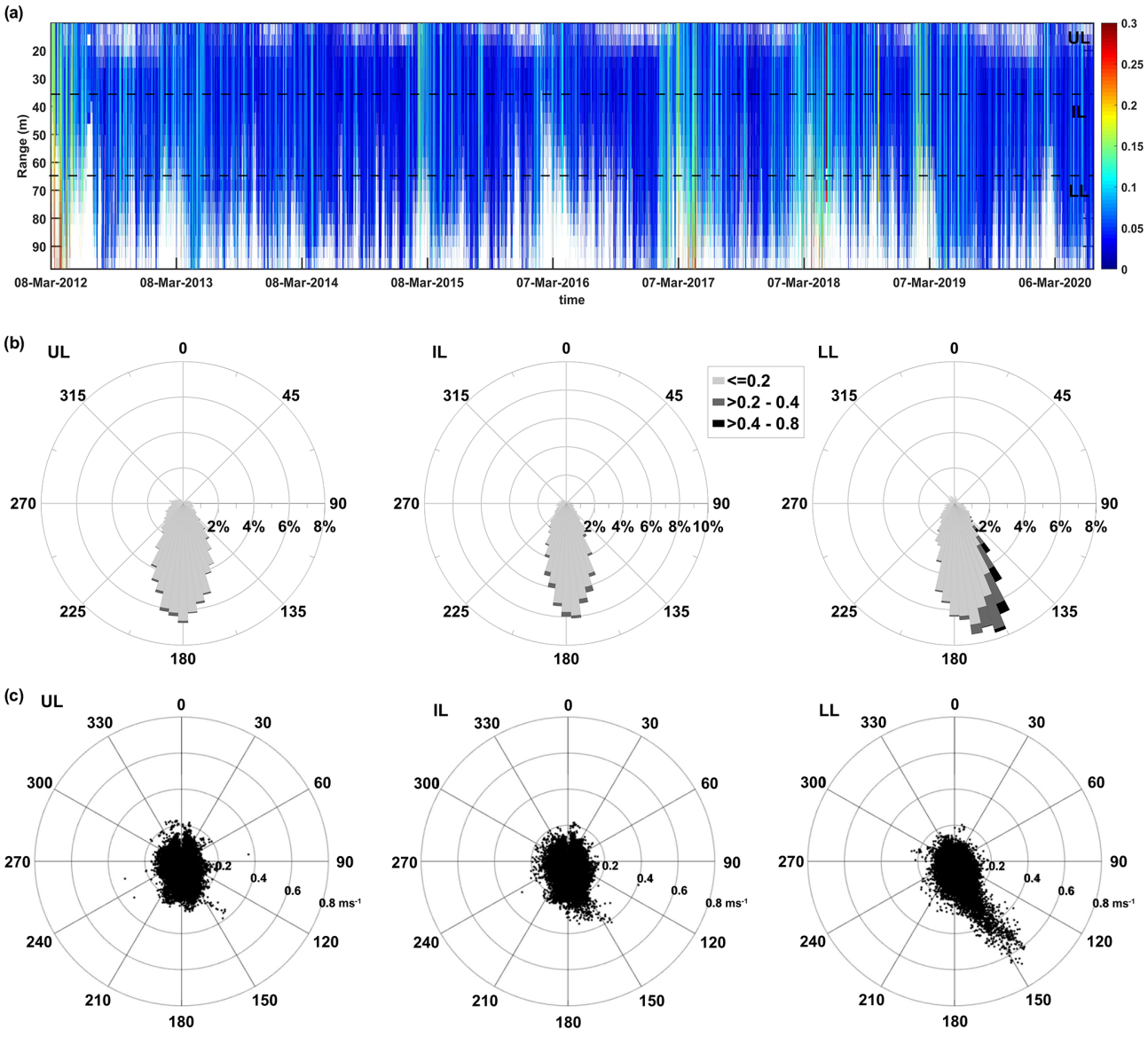

Figure 10. **(a)** Currents' speed records along the water column (data filtered by 80 % percent good), dotted box indicates the water column corresponding to the three layers used for polar plot representation. **(b)** Polar probability plot of current velocity in the three layers of the water column ($m\,s^{-1}$). **(c)** Polar scatterplot of observed directional current velocity ($m\,s^{-1}$) (UL: upper layer; IL: intermediate layer; LL: lower layer) – FF.

($< 0.05\,m\,s^{-1}$), but during the flow acceleration in the bottom layer, its positive values suggest a flow directed toward the seabed.

4 Data availability

All data are made publicly available through the Zenodo repository. The registered database DOI is https://doi.org/10.5281/zenodo.6770201 (Paladini Mendoza, et al., 2022).

This paper describes in detail the temporal coverage of the dataset which is constituted by quite continuous high temporal resolution time series of currents, temperature and salinity from 2012 to 2020. The adopted methodology of mooring configuration and data records and quality control procedures ensures compliance and consistency of the dataset and represents the largest deep-water observatory of current and thermohaline data of the southern Adriatic Sea. The dataset presented concludes in 2020 but monitoring activities are still in progress. Future data collected by these stations will be added to an updated version of the repository as advancing of the data collection to convey the progress of oceanographic observations to the scientific community. The strategy is to have an update of the dataset every 2 years.

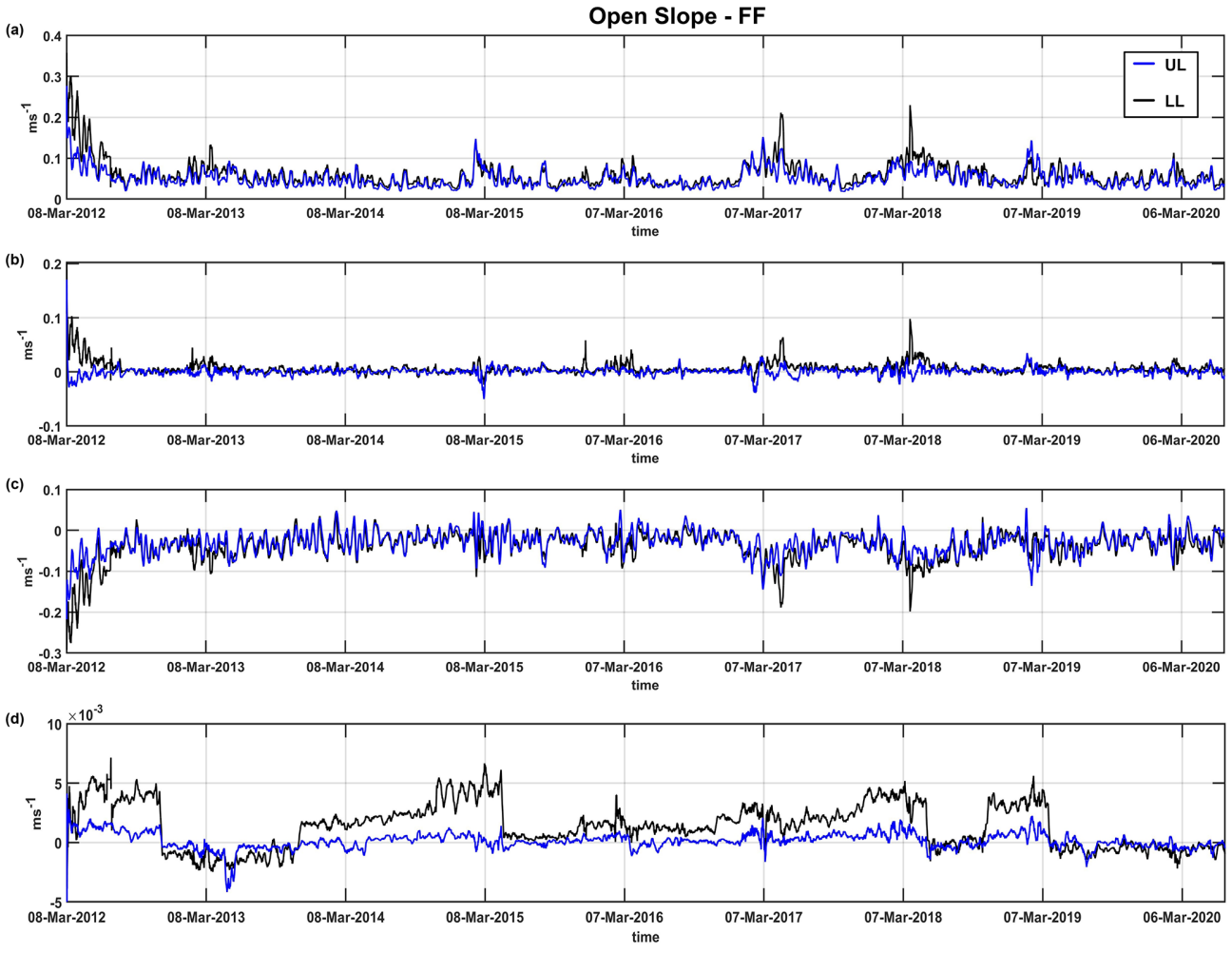

Figure 11. Time series of currents at FF site in the upper (UL) and lower layer (LL) of the water column: **(a)** speed, **(b)** east, **(c)** north and **(d)** vertical components – FF. The data are presented with a 7 d smoothing window.

5 Conclusions

The data presented here are the results of 8 years of monitoring activities conducted on the western margin of the southern Adriatic Sea where two moorings have been placed since 2012 in two sites of the continental slope, representative of two different morpho-dynamic conditions of the southern Adriatic Margin influenced by the passage of dense shelf water.

Long-term high-resolution monitoring in sensitive areas such as zones of dense water passage and deep waters constitutes a key element in the monitoring network of the current context of global climate change, improves the understanding of oceans and sheds light on its complexity. The measurement sites of this dataset represent stable nodes of the European observatory system EMSO-ERIC consortium from 2021. The measurement sites are part of the EMSO's regional facilities for the south Adriatic Sea (managed by CNR-ISP and OGS Trieste) located in the western part of the basin with the objective to assess the Adriatic's response to climate forcing.

The moorings, equipped with ADCP and CTD probes, provide measures of hydrodynamic and thermohaline parameters on a section of the water column extended for the last 100 m from the seabed.

In occasion of the extreme severe cold outbreak in north Adriatic that occurred in 2012, the "Operation Dense Water" was set up, which has produced wide literature about the dynamics of cascading events (in large part, grouped in the special issue edited by Chiggiato et al., 2016b) and their linked processes. The observatory has continued until today with the aim to answer several unaddressed questions. Some open questions are related to the frequency of cascading events and their magnitude variability in a long timescale. This data block extended from 2012 to 2020, to represent a starting point for broadening the knowledge and thus giving even more robustness to previous research results about the southern Adriatic deep-water dynamics.

Generally speaking, the 8-years' time series are characterised in both sites by reigning weak currents ($< 0.1\,m\,s^{-1}$) which undergo yearly to episodic pulsation able to exceed intensity greater than $0.5\,m\,s^{-1}$. These pulsations are linked to the passage of dense waters with low temperature and salinity, which exhibit in both sites an intra- and inter-annual variability. During the year, the oceanographic effects of the passage of these currents are extended over a 6-months window where the core is concentrated between February and May. These dense water masses that originated several months earlier (Vilibic and Orlic, 2002; Vilibic and Supic, 2005; Chiggiato et al., 2016a, b) can flow along the slope in the southern sector until June with a progressive weakening of the intensity. Due to the distance from the generation area, the Adriatic dense water propagation, unlike other sites of dense water generation (i.e. Gulf of Lion), requires more time to reach the southern slope where cascading may occur and the start of passage of dense water flow depends on the onset of the generation. For example, in 2012, first pulses of dense water were observed as early as 3 weeks after its generation in February (Benetazzo et al., 2014).

In the FF site, the flow has a clear dominant direction (140–150° N), especially in the bottom layer. Along the profile, the currents undergo sharp intensification and rotate toward the main direction which takes a definite direction only in the lower layers. The dynamic observed in FF is already described as a peculiar site behaviour where the dense water flow is organised in multiple short-lived pulses with short duration (Chiggiato et al., 2016a). This dynamic leaves traces in the morphology of the FF site where extensive presence of abyssal furrow, documented by Verdicchio et al. (2007), is an indicator of strong and directional currents (Bonaldo et al., 2016) and is oriented (145° N) according to the direction of the currents. The time series can contribute to answer remaining open questions about deep-water dynamics and, in particular, about processes related to dense water passage. The continuous monitoring is fundamental to improve the knowledge about the dense water formation processes, water mass properties, biogeochemical cycles and cascading in the southern Adriatic, and to understand ecosystem function especially in relation to carbon sequestration dynamics and acidification processes in deep waters. In future releases, we plan to include a comparison with other existing data and climatology. The collected parameters are of great interest for different disciplines ranging from geosciences and physical oceanography to biogeochemistry and marine ecology. Recorded variables can be used to compare different sites and other projects can benefit from this monitoring site for the configuration of new monitoring stations.

Author contributions. The long-term monitoring activities were realised by LL, SM, PG and MB. The conceptualisation of the work and its methodology were carried out by FPdM, KS and JC, LL and SM. The data preparation, presentation and analysis were done by FPdM, SM and KS. FPdM, GV and SM created the published database. FPdM wrote the paper, and all co-authors reviewed and contributed to it.

Competing interests. The contact author has declared that none of the authors has any competing interests.

Disclaimer. Publisher's note: Copernicus Publications remains neutral with regard to jurisdictional claims in published maps and institutional affiliations.

Acknowledgements. The authors thank the reviewers for helpful comments that substantially improved the final version of the paper. We are also grateful to the cruise participants, who helped us with the mooring servicing, in particular the captain and the crew members of the R/V *Urania*, R/V *Minerva Uno*, R/V *G. Dallaporta*, R/V *Laura Bassi* and R/V *OGS Explora* as well as the fishing boats *Pasquale & Cristina* and *Attila*.

Financial support. This paper was realised in the context of the PRIN-PASS project (PRIN: Progetti di Ricerca di Rilevante Interesse Nazionale - Bando 2017 - protocol no. 2017ASZAKJ). The maintenance of the BB and FF fixed moorings over time was only possible due to the support of the following projects: the European Community's Seventh Framework Programme projects "Hotspot Ecosystem Research and Man's Impact on European seas" (HERMIONE; grant agreement no. 226354) and "Towards COast to COast NETworks of marine protected areas (from the shore to the high and deep sea), coupled with sea-based wind energy potential" (COCONET; grant agreement no. 287844) as well as the RITMARE (Italian Research for the Sea; grant no. SP5_WP3_AZ1) flagship project. This work was also supported by the EMSO-Italia Joint Research Unit (JRU) and the Ufficio Programmazione e Grant Office of CNR-Italy (CNR-UPGO).

Review statement. This paper was edited by Simona Simoncelli and reviewed by Athanasia Iona and one anonymous referee.

References

Benetazzo, A., Bergamasco, A., Bonaldo, D., Falcieri, F. M., Sclavo, M., Langone, L., and Carniel, S.: Response of the Adriatic Sea to an intense cold air outbreak: dense water dynamics and wave-induced transport, Prog. Oceanogr., 128, 115–138, https://doi.org/10.1016/j.pocean.2014.08.015, 2014.

Bertotti, G., Casolari, E., and Picotti, V.: The Gargano Promontory: a Neogene contractional belt within the Adriatic plate, Terra Nova, 11, 168–173, https://doi.org/10.1046/j.1365-3121.1999.00243.x, 1999.

Bonaldo, D., Benetazzo, A., Bergamasco, A., Campiani, E., Foglini, F., Sclavo, M., Trincardi, F., and Carniel, S.: Interactions among Adriatic continental margin morphology, deep circulation and bedform patterns, Mar. Geol., 375, 82–98, 2016.

Bubbi, A., Cabrini, M., Corbo, A., Fachin, L., Giordano, P., Kuchler, S., Langone, L., Mansutti, P., Miserocchi, S., Reyes Suares, C., Siena, G., Urbini, L., Visnovic, P., and Wirth, A.: Multidisciplinary Approach to Research in Permanent Oceanographic Sites, Cruise Report, FIXO^3 – 09. Cruise Report N. 2020/14 Sez. OCE 4 EXO, 2019.

Cantoni, C., Luchetta, A., Chiggiato, J., Cozzi, S., Schroeder, K., and Langone, L.: Dense water flow and carbonate system in the southern Adriatic: A focus on the 2012 event, Mar. Geol., 375, 15–27, 2016.

Cardin, V., Brunetti, F., Giani, M., Giordano, P., Kovacevic, V., Kuckler, S., Langone, L., Mansutti, P., Canu, D. M., Miserocchi, S., Reyes Suarez, C., Siena, G., Urbini, L., and Visnovic, G.: Multidisciplinary Approach to Research in Permanent Oceanographic Sites, Cruise Report FIXO^3 – 08. Cruise Report N. 2019/10 Sez. OCE 1 EXO, 2018.

Carniel, S., Bonaldo, D., Benetazzo, A., Bergamasco, A., Boldrin, A., Falcieri, F. M., Sclavo, M., Trincardi, F., and Langone, L.: Off-shelf fluxes across the southern Adriatic margin: factors controlling dense-water-driven transport phenomena, Mar. Geol., 375, 44–63, https://doi.org/10.1016/j.margeo.2015.08.016, 2016.

Chiggiato, J., Bergamasco, A., Borghini, M., Falcieri, F. M., Falco, P., Langone, L., Miserocchi, S., Russo, A., and Schroeder, K.: Dense-water bottom currents in the Southern Adriatic Sea in spring 2012, Mar. Geol., 375, 134–145, https://doi.org/10.1016/j.margeo.2015.09.005, 2016a.

Chiggiato, J., Schroeder, K., and Trincardi, F.: Cascading dense shelf-water during the extremely cold winter of 2012 in the Adriatic, Mediterranean Sea: Formation, flow, and seafloor impact – Preface, Mar. Geol., 375, 1–4 2016b.

Civitarese, G., Gačić, M., Cardin, V., and Ibello, V.: Winter Convection Continues in the Warming Southern Adriatic, EOS T. Am. Geophys. Un., 86, 445–451, https://doi.org/10.1029/2005EO450002, 2005.

Foglini, F., Campiani, E., and Trincardi, F.: The reshaping of the South West Adriatic margin by cascading of dense shelf waters, Mar. Geol, 375, 64–81, https://doi.org/10.1016/j.margeo.2015.08.011, 2016.

Franco, P., Jeftić, L., Malanotte-Rizzoli, P., Miehelato, A., and Orlic, M.: Descriptive model of the Northern Adriatic, Oceanol. Acta, 5, 379–389, 1982.

Gačić, M., Civitarese, G., Miserocchi, S., Cardin, V., Crise, A., and Mauri, E.: The open-ocean convection in the Southern Adriatic: a controlling mechanism of the spring phytoplankton bloom, Cont. Shelf. Res., 22, 1897–1908, 2002.

Hald, A.: Statistical theory with engineering applications, John Wiley Sons, New York, ISBN-10 0471340561, 1952.

Hendershott, M. C. and Rizzoli, P.: The winter circulation of the Adriatic Sea, Deep-Sea Res., 23, 353–370, 1976.

Langone, L., Conese, I., Miserocchi, S., Boldrin, A., Bonaldo, D., Carniel, S., Chiggiato, J., Turchetto, M., Borghini, M., and Tesi, T.: Dynamics of particles along the western margin of the Southern Adriatic: processes involved in transferring particulate matter to the deep basin, Mar. Geol., 375, 28–43, https://doi.org/10.1016/j.margeo.2015.09.004, 2016.

Manca, B. B., Kovaĉević, V., Gaĉić, M., and Viezzoli, D.: Dense water formation in the Southern Adriatic Sea and spreading into the Ionian Sea in the period 1997–1999, J. Mar. Syst., 33–34, 133–154, 2002.

Marini, M., Maselli, V., Campanelli, A., Foglini F., and Grilli, F.: Role of the Mid-Adriatic deep in dense water interception and modification, Mar. Geol., 375, 5–14, https://doi.org/10.1016/j.margeo.2015.08.015, 2016.

Martorelli, E., Falcini, F., Salusti, E., and Chiocci, F.: Analysis and modeling of contourite drifts and contour currents off promontories in the Italian Seas (Mediterranean Sea), Mar. Geol., 278, 19–30, 2010.

Mihanović, H., Vilibić, I., Carniel, S., Tudor, M., Russo, A., Bergamasco, A., Bubić, N., Ljubešić, Z., Viličić, D., Boldrin, A., Malačič, V., Celio, M., Comici, C., and Raicich, F.: Exceptional dense water formation on the Adriatic shelf in the winter of 2012, Ocean Sci., 9, 561–572, https://doi.org/10.5194/os-9-561-2013, 2013.

Minisini, D., Trincardi, F., and Asioli, A.: Evidence of slope instability in the Southwestern Adriatic Margin, Nat. Hazards Earth Syst. Sci., 6, 1–20, https://doi.org/10.5194/nhess-6-1-2006, 2006.

Paladini de Mendoza, F., Schroeder, K., Langone, L., Chiggiato, J., Borghini, M., Giordano, P., Verazzo, G., and Miserocchi, S.: Moored current and temperature measurements in the Southern Adriatic Sea at mooring site BB and FF, March 2012–June 2020, Zenodo [data set], https://doi.org/10.5281/zenodo.6770201, 2022.

Ravaioli, M., Bergami, C., Riminucci, F., Langone, L., Cardin, V., Di Sarra, A., Aracri, S., Bastianini, M., Bensi, M., Bergamasco, A., Bommarito, C., Borghini, M., Bortoluzzi, G., Bozzano, R., Cantoni, C., Chiggiato, J., Crisafi, E., D'Adamo, R., Durante, S., Fanara, C., Grilli, F., Lipizer, M., Marini, M., Miserocchi, S., Paschini, E., Penna, P., Pensieri, S., Pugnetti, A., Raicich, F., Schroeder, K., Siena, G., Specchiulli, A., Stanghellini, G., Vetrano, A., and Crise, A.: The RITMARE Italian Fixed-Point Observatory Network (IFON) for marine environmental monitoring: a case study, J. Oper. Oceanogr., 9, s202–s214, https://doi.org/10.1080/1755876X.2015.1114806, 2016.

Ridente, D. and Trincardi, F.: Eustatic and tectonic control on deposition and lateral variability of Quaternary regressive sequences in the Adriatic basin (Italy), Mar. Geol., 184, 273–293, 2002.

Rubino, A., Romanenkov, D., Zanchettin, D., Cardin, V., Hainbucher, D., Bensi, M., Boldrin, A., Langone, L., Miserocchi, S., and Turchetto, M.: On the descent of dense water on a complex canyon system in the southern Adriatic basin, Cont. Shelf Res., 44, 20–29, 2012.

Schroeder, K., Millot, C., Bengara, L., Ben Ismail, S., Bensi, M., Borghini, M., Budillon, G., Cardin, V., Coppola, L., Curtil, C., Drago, A., El Moumni, B., Font, J., Fuda, J. L., García-Lafuente, J., Gasparini, G. P., Kontoyiannis, H., Lefevre, D., Puig, P., Raimbault, P., Rougier, G., Salat, J., Sammari, C., Sánchez Garrido, J. C., Sanchez-Roman, A., Sparnocchia, S., Tamburini, C., Taupier-Letage, I., Theocharis, A., Vargas-Yáñez, M., and Vetrano, A.: Long-term monitoring programme of the hydrological variability in the Mediterranean Sea: a first overview of the HYDROCHANGES network, Ocean Sci., 9, 301–324, https://doi.org/10.5194/os-9-301-2013, 2013.

SeaDataNet: Data Quality Control Procedures, 6th Framework of EC DG Research, Version 2.0, May 2010, https://www.seadatanet.org/Standards/Data-Quality-Control (last access: 7 December 2022), 2010.

Tanhua, T., Pouliquen, S., Hausman, J., O'Brien, K., Bricher, P., de Bruin, T., Buck Justin, J. H., Burger, E. F., Carval, T., Casey Kenneth, S., Diggs, S., Giorgetti, A., Glaves, H., Harscoat, V., Kinkade, D., Muelbert, J. H., Novellino, A., Pfeil, B., Pulsifer, P. L., Van de Putte, A., Robinson, E., Schaap, D., Smirnov, A., Smith, N., Snowden, D., Spears, T., Stall, S., Tacoma, M., Thijsse, P., Tronstad, S., Vandenberghe, T., Wengren, M., Wyborn, L., and Zhao, Z.: Ocean FAIR Data Services, Front. Mar. Sci., 6, 440, https://doi.org/10.3389/fmars.2019.00440, 2019.

Trincardi, F., Verdicchio, G., and Miserocchi, S.: Seafloor evidence for the interaction between cascading and along-slope bottom water masses, J. Geophys. Res., 112, F03011, https://doi.org/10.1029/2006JF000620, 2007a.

Trincardi, F., Foglini, F., Verdicchio, G., Asioli, A., Correggiari, A., Minisini, S., Piva, A., Remia, A., Ridente, D., and Taviani, M.: The impact of cascading currents on the Bari Canyon System, SW-Adriatic Margin (Central Mediterranean), Mar. Geol., 246, 208–23, 2007b.

Turchetto, M., Boldrin, A., Langone, L., Miserocchi, S., Tesi, T., and Foglini, F.: Particle transport in the Bari Canyon (southern Adriatic Sea), Mar. Geol., 246, 231–247, https://doi.org/10.1016/j.margeo.2007.02.007, 2007.

Verdicchio, G. and Trincardi, F.: Short-distance variability in slope bed-forms along the Southwestern Adriatic Margin (Central Mediterranean), Mar. Geol., 234, 271–292, 2006.

Verdicchio, G., Trincardi, F., and Asioli, A.: Mediterranean bottom-current deposits: an example from the Southwestern Adriatic Margin, Geol. Soc. Lond. Spec. Publ., 276, 199–224, 2007.

Vilibić, I. and Orlić, M.: Adriatic water masses, their rates of formation and transport through the Otranto Strait, Deep-Sea Res. Pt. I, 49, 1321–1340, 2002.

Vilibic, I. and Supic, N.: Dense water generation on a shelf: the case of the Adriatic Sea, Ocean Dynam., 55, 403–415, 2005.